Trapping and manipulating single-electron qubits on solid neon in a hybrid circuit quantum electrodynamics architecture

Xianjing Zhou,[1] Gerwin Koolstra,[2] Xufeng Zhang,[1] Ge Yang,[3] Xu Han,[1] Brennan Dizdar,[4] Divan Ralu,[1] Wei Guo,[5,6] Kater W. Murch,[7,*] David I. Schuster,[4,8] and Dafei Jin[1,†]

[1] *Center for Nanoscale Materials, Argonne National Laboratory, Argonne, Illinois 60439, USA*
[2] *Computational Research Division, Lawrence Berkeley National Laboratory, Berkeley, California 94720, USA*
[3] *Laboratory for Nuclear Science, Massachusetts Institute of Technology, Cambridge, Massachusetts 02139, USA*
[4] *James Franck Institute and Department of Physics, University of Chicago, Chicago, Illinois 60637, USA*
[5] *National High Magnetic Field Laboratory, Tallahassee, Florida 32310, USA*
[6] *Department of Mechanical Engineering, FAMU-FSU College of Engineering, Florida State University, Tallahassee, Florida 32310, USA*
[7] *Department of Physics, Washington University in St. Louis, St. Louis, Missouri 63130, USA*
[8] *Pritzker School of Molecular Engineering, University of Chicago, Chicago, Illinois 60637, USA*

(Dated: August 8, 2021)

The promise of quantum computing has driven a persistent quest for new qubit platforms with long coherence, fast operation, and large scalability [1–4]. Electrons, ubiquitous elementary particles of nonzero charge, spin, and mass, have commonly been perceived as paradigmatic local quantum information carriers. Despite superior controllability and configurability, their practical performance as qubits via either motional or spin states depends critically on their material environment [4–7]. Here we report our experimental realization of a new qubit platform based upon isolated single electrons trapped on an ultraclean solid neon surface in vacuum [8–12]. By integrating an electron trap in a circuit quantum electrodynamics architecture [13–20], we achieve strong coupling between the motional states of a single electron and a single microwave photon in an on-chip superconducting resonator. Qubit gate operations and dispersive readout are implemented to measure the energy relaxation time T_1 of 15 μs and phase coherence time T_2 over 200 ns. These results indicate that the electron-on-solid-neon qubit already performs near the state of the art as a charge qubit [21].

The rapid growth of quantum information science and technology in recent years accompanies the remarkable success of various qubit platforms in various domains of quantum information processing. Notable examples include superconducting quantum circuits [14–16,22–27], semiconductor quantum dots [28–37], electromagnetically trapped ions [38–41], optically trapped atoms [42–45], natural or implanted defects [46–52], and magnetic molecules [53–56]. Among different quantum information carriers, isolated single electrons — paradigmatic charged spin-$\frac{1}{2}$ massive particles that naturally interact with photons via quantum electrodynamics (QED) — offer conceivably the straightest approach for efficient manipulation and remote entanglement. So far, electron qubits have been made predominantly in semiconductor heterojunctions and semiconductor-oxide interfaces [4–7]. Despite standardized device fabrication and convenient electrical control, a major challenge faced by these electron qubits is the limited coherent time due to material imperfections or background noise [4–7]. In this circumstance, a new type of single-electron qubit, embedded in an ultraclean low-noise environment, may open up unprecedented opportunities to resolve the coherence challenge. Along with the inherent features of fast operation and large scalability, this single-electron qubit platform holds great potential for development into an ideal quantum computing architecture in the future.

In this work, we demonstrate a fundamentally new solid-state single-electron qubit platform based upon trapping and manipulating isolated single electrons on an ultraclean solid neon surface in vacuum. By integrating the electron trap in a hybrid circuit QED architecture [57–61], we observe vacuum Rabi splitting between the motional state of a single electron and a single microwave photon in an on-chip superconducting resonator. This observation lays the foundation for the quantum coherent control and (single-shot) dispersive readout of electron charge (motional-state) qubits at microwave frequencies in this system. By detuning the electron transition frequency with respect to the resonator frequency, we perform complete qubit characterization, *i.e.*, two-tone qubit spectroscopy [62] and time-domain measurements [63], including Rabi oscillations, T_1 energy relaxation time, and T_2 phase coherence time measurements. Without optimization, the measured $T_1 = 15\,\mu$s and $T_2 \gtrsim 200$ ns have already reached the state of the art for a charge qubit [21], highlighting the promise of this new material environment. With projected development employing spin-charge conversion [17,30,34], we anticipate the nearly perfect spinless environment formed by solid neon [64] to support electron spin qubits with estimated coherence time over 1 s [17,20,65,66]. Beyond quantum computing, this novel solid-state single-electron qubit platform creates an appealing hybrid quantum framework that can connect

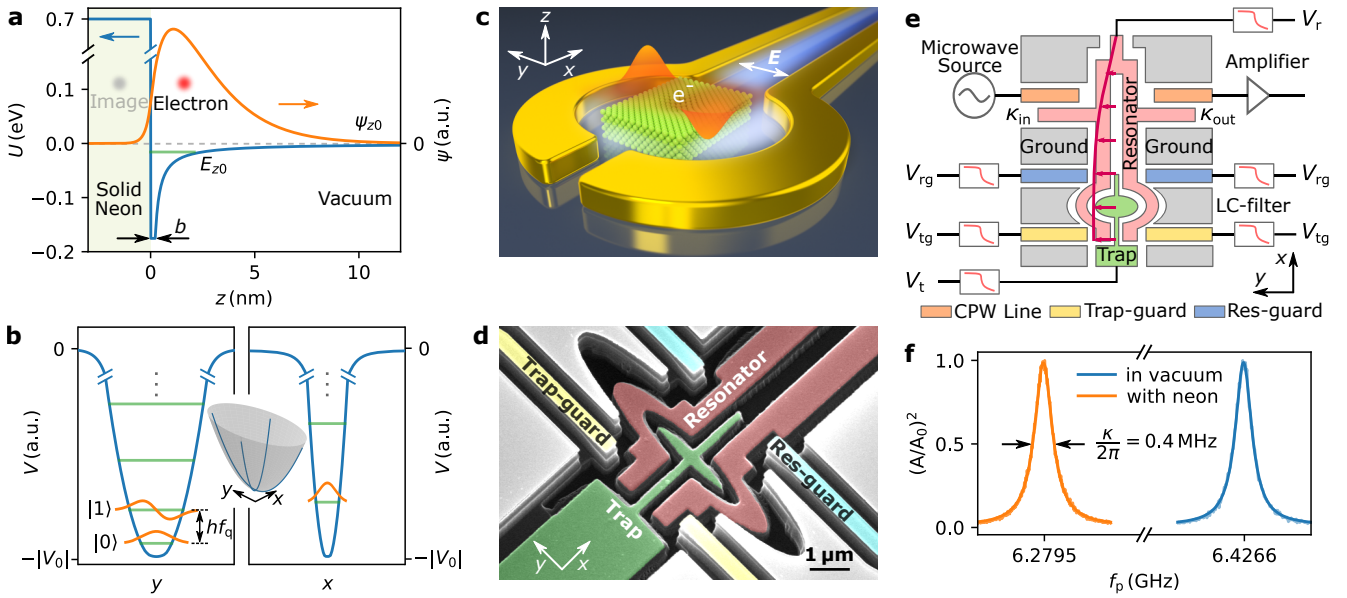

Fig. 1. Electronic structure and device design of the single-electron circuit quantum electrodynamics architecture on solid neon. **a**, Potential energy seen by an excess electron approaching a flat solid neon surface and calculated ground-state eigen-energy and wavefunction in the z-motion. **b**, Schematic of in-plane trapping potential that defines the motional state qubit in y direction. **c**, Conceptual illustration of a single electron trapped on solid neon surface and interacting with microwave photons at the open end of a superconducting coplanar stripline resonator. The electric dipole transition and the electric field of microwave photons are aligned in y direction. **d**, Scanning electron microscopy (SEM) picture of the fabricated device around the electron trap and photon coupling region. The trap and two striplines reside inside a 3.5 μm wide and 1.5 μm deep etched channel. **e**, Specific device structure and functionalities of different components. The quarter-wave superconducting stripline resonator is arranged into a transmission measurement by the input and output capacitive coupling ($\kappa_{\rm in}$ and $\kappa_{\rm out}$ respectively) to coplanar waveguides (CPWs). The electric field of the microwave photons (of the selected antisymmetric mode) between the two striplines has its maximum at the open end. The resonator is biased with a DC voltage $V_{\rm r}$ to control the number of electrons in the reservoir. Three additional DC electrodes (trap, trap-guard, res-guard), biased with the voltages $V_{\rm t}$, $V_{\rm tg}$, $V_{\rm rg}$, control the single-electron trapping and frequency detuning. Each electrode has its own on-chip low-pass LC filter. **f**, Measured resonance peaks before ($f_{\rm r}$ = 6.4266 GHz) and after ($f_{\rm r}$ = 6.2795 GHz) neon fully fills the channel, showing the fitted resonator linewidth $\kappa/2\pi$ = 0.4 MHz.

various qubit platforms, thereby paving new pathways in quantum information science and technology.

Electronic structure and device design

Neon (Ne) is a noble-gas element next to helium (He) in the periodic table. In contrast to He, which is a liquid (superfluid) even at zero temperature, unless a large pressure of at least 25 bar is applied, Ne spontaneously turns into a face-centered-cubic (fcc) crystal after passing its triple point at the elevated temperature $T_{\rm t}$ = 24.556 K and moderate pressure $P_{\rm t}$ = 0.43 bar [67–70]. At near-zero temperature, solid Ne can form a free surface to vacuum and serve as an ultraclean substrate with no uncontrollable impurities or electromagnetic noise [71,72].

When an excess electron approaches a semi-infinite solid Ne surface at $z = 0$ from vacuum, two effects lead to an out-of-plane trapping potential that can bind the electron to the surface (see Fig. 1a). A repulsive barrier, $U \approx 0.7$ eV, occurs due to the Pauli exclusion between the excess electron and atomic shell electrons. In addition, an attractive polarization potential, $V(z) = -(\epsilon-1)/[(\epsilon+1)e^2/4z], (z > b)$, with a dielectric constant $\epsilon = 1.244$ and short-range cutoff $b \approx 2.3$ Å, occurs due to the induced image charge inside solid Ne [8,9,20,73]. With this potential, the electron's z-motion has a ground-state energy $E_{z0} = -15.8$ meV and an eigen-wavefunction peaked at about 1 nm distance from the surface (Fig. 1a). The energy cost to bring the electron to the first excited state in z is 12.7 meV, equivalent to a 147 K activation temperature. Therefore, at our 10 mK experimental temperature, the electron is frozen within the ground-state subband of z-motion. Previous studies have verified that solid Ne surface can hold a nondegenerate two-dimensional electron gas with $\sim 10^{10}$ cm^{-2} high density and $\sim 10^4$ cm^2 V^{-1} s^{-1} high mobility [74].

Condensed (liquid or solid) noble-gas elements with positive (repulsive) electron affinity are the only materials in nature that can hold electrons on a free surface in vacuum. Practically, all other materials, even electronically insulating and atomically smooth, have negative (attractive) electron affinity and contain charged contaminants or dangling bonds on the surface that can capture and localize excess electrons at atomic to molecular scales [75,76]. While the electron-on-solid-Ne (eNe) system can be considered conceptually as an

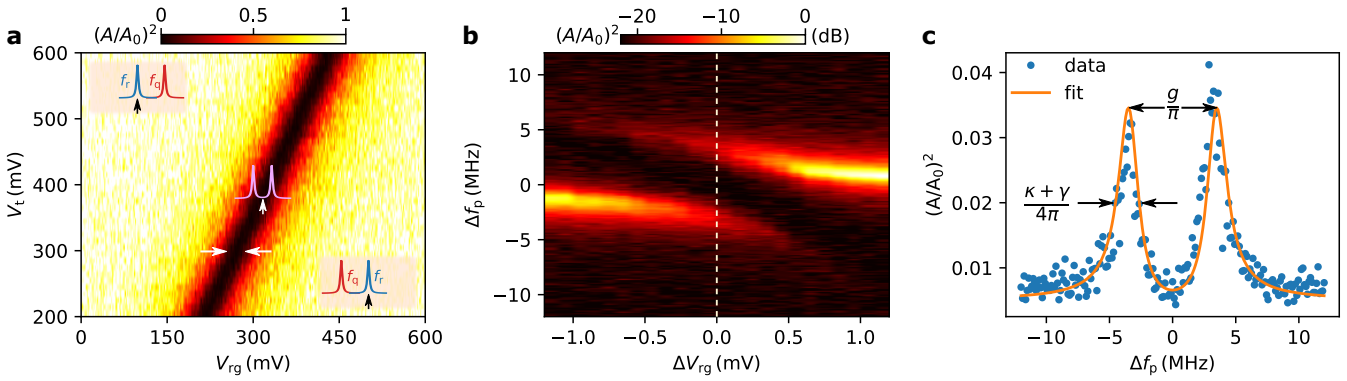

Fig. 2. Strong coupling and vacuum Rabi splitting between a single electron on solid neon and a single microwave photon in a superconducting resonator. **a**, Normalized microwave transmission amplitude $(A/A_0)^2$ probed at the resonator frequency f_r (black and white vertical arrows in the insets) versus the trap voltage V_t and the resonator-guard voltage V_{rg}. The amplitude drops when the electron's transition frequency f_q is tuned on resonance with the resonator. **b**, Normalized $(A/A_0)^2$ versus probe frequency $\Delta f_p = f_p - f_r$ and resonator-guard voltage ΔV_{rg} (detuning from the resonance condition) in the region indicated by the white horizontal arrows in (**a**) with fixed V_t. **c**, Line cut from (**b**) along the white dashed line when the qubit frequency f_q is on resonance with the resonator frequency f_r. The two peaks show the vacuum Rabi splitting, giving the coupling strength $g/2\pi = 3.5$ MHz and intrinsic electron linewidth $\gamma/2\pi = 1.7$ MHz, fitted by input-output theory with the known resonator linewidth $\kappa/2\pi = 0.4$ MHz.

extension to the historically more studied electron-on-liquid-He (eHe) system, it exhibits much stronger surface rigidity that suppresses decoherence through surface excitations [17–19]. Compared with eHe that was proposed as a qubit platform over two decades ago [11,17–19,77–79], eNe embodies a potentially transformative solid-state qubit platform [12,20,71].

On a flat Ne surface, the electron takes plane-wave eigenstates in the xy plane. To confine the electron in the plane, we utilize carefully designed lateral trapping electrodes to hold the electrons individually and deterministically in space [19], with trapping time exceeding two months. We tune the electrode voltages to further constrain the electron's x-motion to its ground state and take the two lowest energy states of y-motion as the qubit states (see Fig. 1b). Figure 1c shows a simplified conceptual illustration of our arrangement of the trapped electron and microwave resonator. The electron is on the solid Ne surface at the open end (in a "clamp" shape) of a quarter-wave coplanar double-stripline resonator [19,80]. The electric field (of the selected antisymmetric mode) is strongest there, and its direction is aligned with electron's y-motion, perpendicular to the extending direction of the striplines in x. Figure 1d displays a scanning electron microscopy (SEM) image of the actual device structure around the trapping area. All the metal lines and ground planes are made of superconducting niobium (Nb) deposited on a high-resistivity silicon substrate. A "trap" electrode, applied with positive voltage, plugs into the open end of the "resonator". Four "guard" electrodes, named as "trap guards" and "res(onator) guards" surrounding the trap, applied with voltages in pairs, provide precise tuning to the trapping potential and thus the electron transition frequency about the resonator frequency. The trap and resonator reside inside a ~ 4 mm long etched channel.

Figure 1e illustrates in more details about this hybrid circuit QED device. The double stripline resonator is coupled with coplanar waveguides (CPWs) with the input and output coupling rate κ_{in} and κ_{out}, respectively, in a transmission measurement configuration. Each DC electrode, biased at V_r, V_t, V_{rg}, V_{tg}, respectively, has its own on-chip low-pass LC filter that isolates the electron and resonator from the DC electrodes at microwave frequencies to protect the qubit lifetime and resonator qualify factor. We fill liquid Ne into the experimental cell at 26 K and cool down to 10 mK. The shift of resonator frequency f_r can be used to infer Ne thickness. When the channel is fully filled with Ne, f_r shifts from 6.4266 GHz to 6.2795 GHz (see Fig. 1f). In practice, we only put in a tiny amount of Ne to coat the device surface, resulting only 0.3–0.6 MHz frequency shift and 5–10 nm estimated Ne thickness from numerical simulation. The observed resonator linewidth $\kappa/2\pi = 0.4$ MHz, independent of Ne filling, indicates a quality factor $Q \approx 1.6 \times 10^4$. Electrons are generated through thermionic emission from a pair of tungsten filaments inside the cell under a voltage pulse train (width: 0.1 ms, height: 4 V, and repetition rate: 1 kHz) for a total duration of 1 s [18,19]. (See Supplementary Information (SI) for more details.)

Strong coupling and vacuum Rabi splitting

We use a similar scheme in our previous work [19] to load single electrons onto the trap from the channel hosting the stripline resonator, and in the meanwhile, monitor the microwave transmission signal. Once an electron is trapped, we fix the resonator voltage V_r at 1 V and trap-guard voltage V_{tg} at 0 V. A positive V_r is necessary to keep any remnant electrons inside the

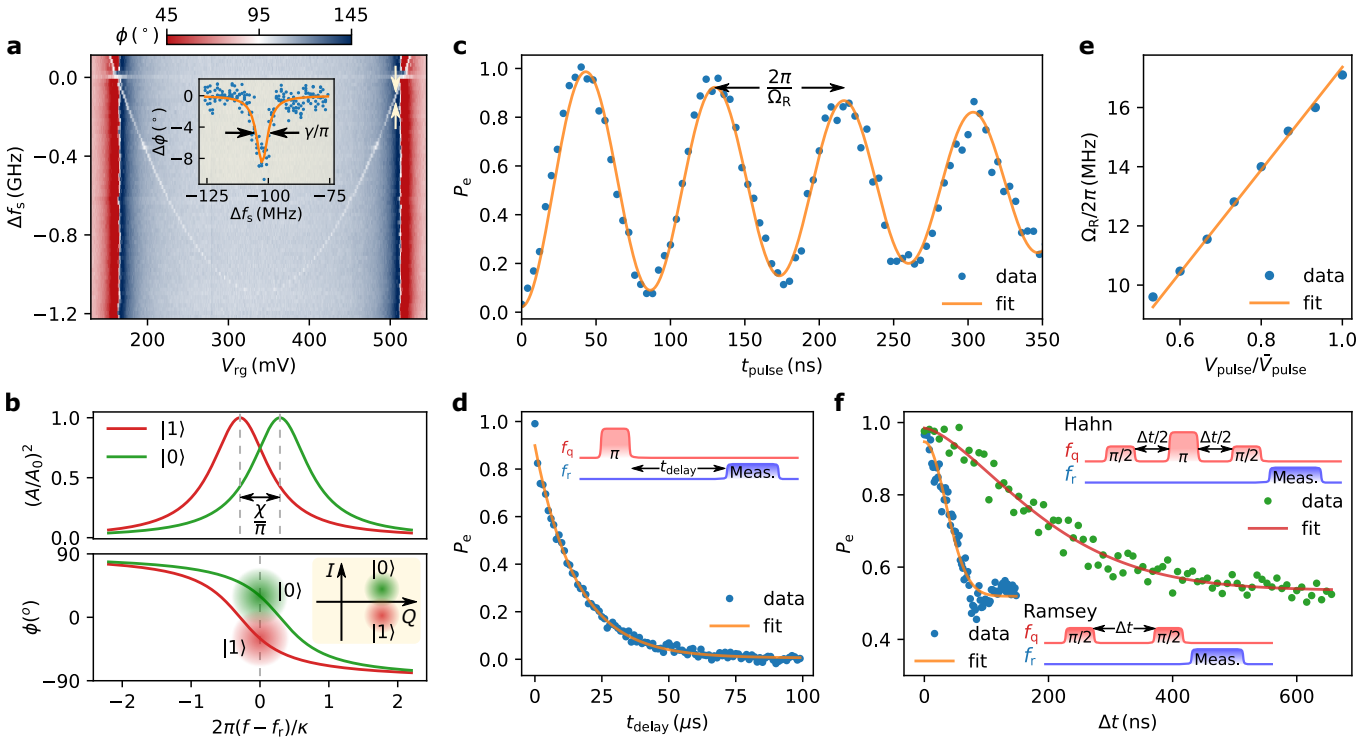

Fig. 3. Spectroscopy and time-domain characterization of a single-electron qubit on solid neon. **a**, Two-tone qubit spectroscopy measurement on the transmission phase ϕ at the resonator frequency f_r versus the detuned drive frequency $\Delta f_s = f_s - f_r$ and the resonator-guard voltage V_{rg}. The qubit linewidth γ can be obtained by fitting the phase dip profile (inset). **b**, Illustration of the dispersive readout of single-electron qubit state by transmission measurement. Ground and excited electron states cause the actual resonator frequency to be blueshifted and redshifted and the measured transmission phase ϕ at the bare resonator frequency f_r to show on average $\pm 30°$ shift. **c**, Rabi oscillations of the excited state population P_e, measured at fixed pulse amplitude and varied pulse length t_{pulse}. **d**, Qubit relaxation measurement with the fitted relaxation time $T_1 = 15\,\mu$s. **e**, Measured linear dependence of Rabi frequency Ω_R on the amplitude of gate pulses. **f**, Ramsey fringe and Hahn echo measurements with the fitted original coherence time $T_2^* = 50$ ns and extended coherence time $T_{2E} = 220$ ns. Qubit detuning for (**b**) – (**f**) is kept at $\Delta/2\pi \equiv f_q - f_r = -100$ MHz.

long channel far off resonance. The trap voltage V_t and resonator-guard voltage V_{rg} are enough to tune the qubit frequency f_q into resonance with the resonator frequency $f_r \approx 6.426$ GHz. Figure 2a gives a color plot of the normalized transmission amplitude $(A/A_0)^2$ probed at the resonator frequency f_r versus the tuning voltages V_t and V_{rg} for a trapped electron. When f_q is tuned across f_r, we observe a sharp drop in the microwave transmission amplitude probed at f_r [14]. The average photon occupancy in the resonator is controlled at the single-photon level, $\bar{n} \approx 1$, with about -135 dBm input power to the resonator. (See SI for more details.)

By measuring the transmission spectrum as a function of probe frequency f_p near the resonator frequency f_r, we observe a clear avoided crossing – vacuum Rabi splitting, when V_t is fixed and V_{rg} tunes the qubit frequency across the resonator frequency (see Fig. 2b). Figure 2c shows the line cut of Fig. 2b in the on-resonance case $f_q = f_r$. A fit over the two peaks by input-output theory [81] yields the coupling strength $g/2\pi = 3.5$ MHz, which is nearly twice of the electron dephasing rate $\gamma/2\pi \approx 1.7$ MHz, with the known resonator decay rate $\kappa/2\pi \approx 0.4$ MHz. (See SI for more details.) The system has clearly entered the strong coupling regime [14], $g > \gamma, \kappa$, which instantly enables coherent microwave control and dispersive readout of single-electron qubits in this system.

Spectroscopy and time-domain characterization

Figure 3a shows a two-tone qubit spectroscopy measurement of *another* trapped electron. The qubit frequency f_q is tuned by the resonator-guard voltage V_{rg}. At each given V_{rg}, we monitor the transmission phase ϕ at the bare resonator frequency f_r while a probe tone f_s is slowly swept over a range of ~ 1 GHz across the qubit frequency f_q. When f_s is resonant with f_q, it partially excites the qubit, inducing a dip ($f_q < f_r$) or a peak ($f_q > f_r$) in the ϕ versus f_s plot (Fig. 3a inset). By scanning both f_s and V_{rg}, we obtain the intrinsic qubit spectrum as a function of V_{rg}. A Lorentzian fit of this qubit spectrum yields the linewidth $\gamma/2\pi = 2.8$ MHz. The probe-tone power is kept low enough here to avoid power broadening of the qubit over its natural linewidth. The overall spectrum resembles that of a double-quantum-dot qubit (DQD) spectrum at a semiconductor interface [32,33]. (See SI for more discussion.)

By increasing the probe-tone power, we investigate the anharmonicity under a varied detuning $\Delta/2\pi \equiv f_q - f_r$ between ± 100 MHz. At -100 MHz detuning, the measured anharmonicity between the two lowest transition frequencies is $\alpha/2\pi \equiv f_{|1\rangle\to|2\rangle} - f_{|0\rangle\to|1\rangle} \approx 40$ MHz, where $|0\rangle$, $|1\rangle$, $|2\rangle$ are the ground, first-excited, and second-excited states, respectively (see SI). This α is positive and consistent with the value expected from the trap design [19]. Even though this α value currently limits single qubit gate durations to $t_\pi \gg \pi/\alpha \approx 12$ ns, it can be easily enhanced in future trap designs.

The measured coupling strength for this electron is $g/2\pi = 4.5$ MHz (see SI). At large detuning $\Delta/2\pi = -100$ MHz, we have $|\Delta| \gg g$. The dispersive coupling between the qubit and resonator provides a qubit-state-dependent frequency shift $\chi \approx g^2\alpha/\Delta(\Delta+\alpha)$ [25]. By measuring the transmission phase ϕ of the photons at f_r, we can read out the qubit state [62]. Figure 3b illustrates the scheme of dispersive readout in accordance with our experiment, as is common in circuit QED platforms [63,82]. The measured ϕ shift at f_r is about $\pm 30°$ after statistical average, corresponding to $\chi/2\pi \approx 0.12$ MHz. Ideally, the qubit would operate at the spectrum minimum of Fig. 3a, *i.e.*, the "sweet spot" where the charge noise has the lowest effect. However, for this particular electron at the "sweet spot", the > 1 GHz large detuning precludes state readout with reasonable signal-to-noise ratio.

We now use real-time coherent control to measure the coherence properties of the qubit at $\Delta/2\pi = -100$ MHz detuning. Figure 3c displays Rabi oscillations in the excited-state population P_e [83]. Starting with the qubit in its ground state, we apply a pulse with variable duration and fixed amplitude at the qubit frequency f_q, immediately followed by a readout pulse applied at the resonator frequency f_r. Figure 3d displays the results of a T_1 relaxation time measurement, where we utilize a π-pulse (duration inferred from Fig. 3c) and vary the delay t_{delay} between the end of each π-pulse and the onset of readout pulse. The exponential decay signifies a long $T_1 = 15\,\mu$s compared with most semiconductor charge qubits [21]. We also verify the linear dependence of Rabi frequency Ω_R on the pulse amplitude V_{pulse} normalized by the maximally used amplitude $\bar{V}_{pulse}$ (see Fig. 3e).

Figure 3f shows the measurements of the original (Ramsey fringe) coherence time T_2^* and extended (Hahn echo) coherence time T_{2E} [83]. The Ramsey fringe measurement consists of two $\pi/2$ pulses separated by a varied delay time Δt. A fit over the population curve yields $T_2^* = 50$ ns, consistent with the linewidth inferred from two-tone spectroscopy. This measurement, however, is sensitive to the dephasing due to slow electromagnetic fluctuations in the circuit. The Hahn echo measurement inserts an additional π pulse in the middle point between two $\pi/2$ pulses. A fit yields an extended echo coherence time $T_{2E} = 220$ ns, suggesting that the qubit coherence is affected by low-frequency charge noise. (See SI for more details.)

Discussion and outlook

The long T_1 manifests that solid Ne can indeed serve as an ultraclean substrate for single-electron qubits. We expect future trap geometries and better filtering for DC electrodes to give even longer T_1. The still short $T_2 \ll T_1$ at this initial stage of development may originate from two sources of residual charge noise. First, remnant electrons along the resonator in the long channel are not entirely fixed; remaining motion can cause background charge noise to the trapped electron-photon interacting system. Second, residual roughness of the Ne surface may cause extra scattering to the electron motion. Improvement to the device design and Ne growth process [66], and operation at the charge noise "sweet spot" are expected to mitigate these decoherence issues. It has been theoretically calculated that the in-plane motional coherence of an electron on solid Ne surface can be several milliseconds [71]. Ultimately, utilizing the spin states through engineered spin-orbital coupling [17,30,34] can yield ultralong qubit coherence in excess of 1 s [17,20,65,66].

The strong interaction between the electron motional states and microwave photons will allow two or more electrons to entangle with each other through exchanging (virtual) photons in the resonator [26,84]. To scale the system up, we can adopt the quantum charge-coupled device (QCCD) technique, originally developed in the trapped ion system [41,78,85], to shuffle electrons into and out of different functional zones on a chip to achieve multi-electron gating, entanglement, and readout. This will significantly expand the scalability.

The eNe qubit platform incorporates compelling advantages from several leading qubit platforms; analogous to electromagnetically trapped ions, the electron qubits here are identically generated by a simple source and can have long spin coherence times; as with semiconductor quantum dots, electronic gate control can be applied at high speed; finally, strong coupling with the circuit QED architecture enables dispersive readout, transduction to microwave photons, and two-qubit gates via microwave resonator mediated interactions. Given these merits, we anticipate the eNe qubit platform to rapidly evolve into a superior quantum computing hardware. Furthermore, it can be coherently linked with other quantum information systems, *e.g.*, Josephson junctions and color centers through microwaves, to collectively advance quantum sensing, transduction, networks, and other important areas in quantum science, as well as fundamental physics.

ACKNOWLEDGMENTS

This work was performed at the Center for Nanoscale Materials, a U.S. Department of Energy Office of Science User Facility, and supported by the U.S. Department of Energy, Office of Science, under Contract No. DE-AC02-06CH11357. D. J. acknowledges support from Argonne National Laboratory Directed Research and Development (LDRD) and Julian Schwinger Foundation

for Physics Research. D. I. S. and B. D. acknowledge support from NSF DMR grant DMR-1906003. This work was partially supported by the University of Chicago Materials Research Science and Engineering Center, which is funded by the National Science Foundation under award number DMR-2011854. This work made use of the Pritzker Nanofabrication Facility of the Institute for Molecular Engineering at the University of Chicago, which receives support from SHyNE, a node of the National Science Foundations National Nanotechnology Coordinated Infrastructure (NSF NNCI-1542205). K. W. M acknowledges support from NSF Grant No. PHY-1752844 (CAREER) and use of facilities at the Institute of Materials Science and Engineering at Washington University. W. G. acknowledges support from the National Science Foundation (Grant No. DMR-2100790) and the National High Magnetic Field Laboratory which is funded through the NSF Cooperative Agreement No. DMR-1644779 and the state of Florida. G. Y. is supported by the National Science Foundation under Cooperative Agreement PHY-2019786 (the NSF AI Institute for Artificial Intelligence and Fundamental Interactions). The CNM team acknowledges Greg Calusine, Kyle Serniak, and William Oliver of MIT Lincoln Laboratory for offering traveling wave parametric amplifiers (TWPAs).

* murch@physics.wustl.edu
† djin@anl.gov

[1] D. P. DiVincenzo, Fortschr. Phys. **48**, 771 (2000).
[2] T. D. Ladd, F. Jelezko, R. Laflamme, Y. Nakamura, C. Monroe, and J. L. O'Brien, Nature **464**, 45 (2010).
[3] G. Popkin, Science **354**, 1090 (2016).
[4] N. P. de Leon, K. M. Itoh, D. Kim, K. K. Mehta, T. E. Northup, H. Paik, B. S. Palmer, N. Samarth, S. Sangtawesin, and D. W. Steuerman, Science **372**, 253 (2021).
[5] R. Hanson, L. P. Kouwenhoven, J. R. Petta, S. Tarucha, and L. M. Vandersypen, Rev. Mod. Phys. **79**, 1217 (2007).
[6] F. A. Zwanenburg, A. S. Dzurak, A. Morello, M. Y. Simmons, L. C. Hollenberg, G. Klimeck, S. Rogge, S. N. Coppersmith, and M. A. Eriksson, Rev. Mod. Phys. **85**, 961 (2013).
[7] L. M. K. Vandersypen, H. Bluhm, J. S. Clarke, A. S. Dzurak, R. Ishihara, A. Morello, D. J. Reilly, L. R. Schreiber, and M. Veldhorst, Npj Quantum Inf. **3**, 1 (2017).
[8] M. W. Cole and M. H. Cohen, Phys. Rev. Lett. **23**, 1238 (1969).
[9] M. W. Cole, Rev. Mod. Phys. **46**, 451 (1974).
[10] P. Leiderer, J. Low Temp. Phys. **87**, 247 (1992).
[11] P. Platzman and M. I. Dykman, Science **284**, 1967 (1999).
[12] I. I. Smolyaninov, Int. J. Mod. Phys. B **15**, 2075 (2001).
[13] A. Blais, R.-S. Huang, A. Wallraff, S. M. Girvin, and R. J. Schoelkopf, Physical Review A **69**, 062320 (2004).
[14] A. Wallraff, D. I. Schuster, A. Blais, L. Frunzio, R. S. Huang, J. Majer, S. Kumar, S. M. Girvin, and R. J. Schoelkopf, Nature **431**, 162 (2004).
[15] A. Blais, S. M. Girvin, and W. D. Oliver, Nat. Phys. **16**, 247 (2020).
[16] A. Blais, A. L. Grimsmo, and A. Wallraff, Rev. Mod. Phys. **93**, 25005 (2021).
[17] D. I. Schuster, A. Fragner, M. I. Dykman, S. A. Lyon, and R. J. Schoelkopf, Phys. Rev. Lett. **105**, 040503 (2010).
[18] G. Yang, A. Fragner, G. Koolstra, L. Ocola, D. A. Czaplewski, R. J. Schoelkopf, and D. I. Schuster, Phys. Rev. X **6**, 011031 (2016).
[19] G. Koolstra, G. Yang, and D. I. Schuster, Nat. Commun. **10**, 5323 (2019).
[20] D. Jin, Quantum Sci. Technol. **5**, 035003 (2020).
[21] G. Burkard, M. J. Gullans, X. Mi, and J. R. Petta, Nat. Rev. Phys. **2**, 129 (2020).
[22] Y. Nakamura, Y. A. Pashkin, and J. S. Tsai, Nature **398**, 786 (1999).
[23] Y. Makhlin, G. Schön, and A. Shnirman, Rev. Mod. Phys. **73**, 357 (2001).
[24] I. Chiorescu, Y. Nakamura, C. M. Harmans, and J. Mooij, Science **299**, 1869 (2003).
[25] J. Koch, M. Y. Terri, J. Gambetta, A. A. Houck, D. I. Schuster, J. Majer, A. Blais, M. H. Devoret, S. M. Girvin, and R. J. Schoelkopf, Phys. Rev. A **76**, 042319 (2007).
[26] J. Majer, J. M. Chow, J. M. Gambetta, J. Koch, B. R. Johnson, J. A. Schreier, L. Frunzio, D. I. Schuster, A. A. Houck, A. Wallraff, A. Blais, M. H. Devoret, S. M. Girvin, and R. J. Schoelkopf, Nature **449**, 443 (2007).
[27] F. Arute, K. Arya, R. Babbush, *et al.*, Nature **574**, 505 (2019).
[28] J. R. Petta, A. C. Johnson, J. M. Taylor, E. A. Laird, A. Yacoby, M. D. Lukin, C. M. Marcus, M. P. Hanson, and A. C. Gossard, Science **309**, 2180 (2005).
[29] F. H. Koppens, C. Buizert, K.-J. Tielrooij, I. T. Vink, K. C. Nowack, T. Meunier, L. Kouwenhoven, and L. Vandersypen, Nature **442**, 766 (2006).
[30] E. Kawakami, P. Scarlino, D. R. Ward, F. Braakman, D. Savage, M. Lagally, M. Friesen, S. N. Coppersmith, M. A. Eriksson, and L. Vandersypen, Nat. Nanotechnol. **9**, 666 (2014).
[31] E. Kawakami, T. Jullien, P. Scarlino, D. R. Ward, D. E. Savage, M. G. Lagally, V. V. Dobrovitski, M. Friesen, S. N. Coppersmith, M. A. Eriksson, *et al.*, Proc. Natl. Acad. Sci. **113**, 11738 (2016).
[32] X. Mi, J. V. Cady, D. M. Zajac, P. W. Deelman, and J. R. Petta, Science **355**, 156 (2017).
[33] A. Stockklauser, P. Scarlino, J. V. Koski, S. Gasparinetti, C. K. Andersen, C. Reichl, W. Wegscheider, T. Ihn, K. Ensslin, and A. Wallraff, Phys. Rev. X **7**, 1 (2017).
[34] X. Mi, M. Benito, S. Putz, D. M. Zajac, J. M. Taylor, G. Burkard, and J. R. Petta, Nature **555**, 599 (2018).
[35] N. Samkharadze, G. Zheng, N. Kalhor, D. Brousse, A. Sammak, U. C. Mendes, A. Blais, G. Scappucci, and L. M. Vandersypen, Science **1127**, 1123 (2018).
[36] A. J. Landig, J. V. Koski, P. Scarlino, U. C. Mendes, A. Blais, C. Reichl, W. Wegscheider, A. Wallraff, K. Ensslin, and T. Ihn, Nature **560**, 179 (2018).
[37] L. Petit, H. Eenink, M. Russ, W. Lawrie, N. Hendrickx, S. Philips, J. Clarke, L. Vandersypen, and M. Veldhorst, Nature **580**, 355 (2020).

[38] C. Monroe, D. M. Meekhof, B. E. King, W. M. Itano, and D. J. Wineland, Phys. Rev. Lett. **75**, 4714 (1995).
[39] D. Leibfried, R. Blatt, C. Monroe, and D. Wineland, Rev. Mod. Phys. **75**, 281 (2003).
[40] C. D. Bruzewicz, J. Chiaverini, R. McConnell, and J. M. Sage, Appl. Phys. Rev. **6**, 021314 (2019).
[41] J. M. Pino, J. M. Dreiling, C. Figgatt, J. P. Gaebler, S. A. Moses, M. S. Allman, C. H. Baldwin, M. Foss-Feig, D. Hayes, K. Mayer, C. Ryan-Anderson, and B. Neyenhuis, Nature **592**, 209 (2021).
[42] G. K. Brennen, C. M. Caves, P. S. Jessen, and I. H. Deutsch, Phys. Rev. Lett. **82**, 1060 (1999).
[43] D. Jaksch, J. I. Cirac, P. Zoller, S. L. Rolston, R. Côté, and M. D. Lukin, Phys. Rev. Lett. **85**, 2208 (2000).
[44] M. Saffman, T. G. Walker, and K. Mølmer, Rev. Mod. Phys. **82**, 2313 (2010).
[45] Y. Wang, A. Kumar, T.-Y. Wu, and D. S. Weiss, Science **352**, 1562 (2016).
[46] J. Weber, W. Koehl, J. Varley, A. Janotti, B. Buckley, C. Van de Walle, and D. D. Awschalom, Proc. Natl. Acad. Sci. **107**, 8513 (2010).
[47] A. Morello, J. J. Pla, F. A. Zwanenburg, K. W. Chan, K. Y. Tan, H. Huebl, M. Möttönen, C. D. Nugroho, C. Yang, J. A. Van Donkelaar, A. D. Alves, D. N. Jamieson, C. C. Escott, L. C. Hollenberg, R. G. Clark, and A. S. Dzurak, Nature **467**, 687 (2010).
[48] J. J. Pla, K. Y. Tan, J. P. Dehollain, W. H. Lim, J. J. Morton, D. N. Jamieson, A. S. Dzurak, and A. Morello, Nature **489**, 541 (2012).
[49] J. J. Pla, K. Y. Tan, J. P. Dehollain, W. H. Lim, J. J. Morton, F. A. Zwanenburg, D. N. Jamieson, A. S. Dzurak, and A. Morello, Nature **496**, 334 (2013).
[50] J. T. Muhonen, J. P. Dehollain, A. Laucht, F. E. Hudson, R. Kalra, T. Sekiguchi, K. M. Itoh, D. N. Jamieson, J. C. McCallum, A. S. Dzurak, and A. Morello, Nat. Nanotechnol. **9**, 986 (2014).
[51] S. Chen, M. Raha, C. M. Phenicie, S. Ourari, and J. D. Thompson, Science **370**, 592 (2020).
[52] G. Wolfowicz, F. J. Heremans, C. P. Anderson, S. Kanai, H. Seo, A. Gali, G. Galli, and D. D. Awschalom, Nat. Rev. Mater. (2021).
[53] R. Vincent, S. Klyatskaya, M. Ruben, W. Wernsdorfer, and F. Balestro, Nature **488**, 357 (2012).
[54] S. Thiele, F. Balestro, R. Ballou, S. Klyatskaya, M. Ruben, and W. Wernsdorfer, Science **344**, 1135 (2014).
[55] M. Atzori and R. Sessoli, J. Am. Chem. Soc. **141**, 11339 (2019).
[56] E. Coronado, Nat. Rev. Mater. **5**, 87 (2020).
[57] Y. Kubo, C. Grezes, A. Dewes, T. Umeda, J. Isoya, H. Sumiya, N. Morishita, H. Abe, S. Onoda, T. Ohshima, *et al.*, Phys. Rev. Lett. **107**, 220501 (2011).
[58] R. W. Andrews, R. W. Peterson, T. P. Purdy, K. Cicak, R. W. Simmonds, C. A. Regal, and K. W. Lehnert, Nat. Phys. **10**, 321 (2014).
[59] G. Kurizki, P. Bertet, Y. Kubo, K. Mølmer, D. Petrosyan, P. Rabl, and J. Schmiedmayer, Proc. Natl. Acad. Sci. **112**, 3866 (2015).
[60] K. J. Satzinger, Y. Zhong, H.-S. Chang, G. A. Peairs, A. Bienfait, M.-H. Chou, A. Cleland, C. R. Conner, É. Dumur, J. Grebel, B. H. November, R. G. Povey, S. J. Whiteley, D. D. Awschalom, D. I. Schuster, and A. N. Cleland, Nature **563**, 661 (2018).
[61] A. A. Clerk, K. W. Lehnert, P. Bertet, J. R. Petta, and Y. Nakamura, Nat. Phys. **16**, 257 (2020).
[62] D. I. Schuster, A. Wallraff, A. Blais, L. Frunzio, R. S. Huang, J. Majer, S. M. Girvin, and R. J. Schoelkopf, Phys. Rev. Lett. **94**, 123602 (2005).
[63] A. Wallraff, D. I. Schuster, A. Blais, L. Frunzio, J. Majer, M. H. Devoret, S. M. Girvin, and R. J. Schoelkopf, Phys. Rev. Lett. **95**, 060501 (2005).
[64] The naturally occurring 0.27% abundance of spinful ^{21}Ne can be purified away.
[65] S. A. Lyon, Phys. Rev. A **74**, 052338 (2006).
[66] S. Sheludiakov, J. Ahokas, J. Järvinen, L. Lehtonen, S. Vasiliev, Y. A. Dmitriev, D. M. Lee, and V. V. Khmelenko, J. Low Temp. Phys. **195**, 365 (2019).
[67] R. T. Jacobsen, S. G. Penoncello, and E. W. Lemmon, in *Thermodynamic Properties of Cryogenic Fluids* (Springer, 1997) pp. 31–287.
[68] D. G. Henshaw, Phys. Rev. **111**, 1470 (1958).
[69] G. L. Pollack, Rev. Mod. Phys. **36**, 748 (1964).
[70] D. N. Batchelder, D. L. Losee, and R. O. Simmons, Phys. Rev. **162**, 767 (1967).
[71] V. Zavyalov, I. Smolyaninov, E. Zotova, A. Borodin, and S. Bogomolov, J. Low Temp. Phys. **138**, 415 (2005).
[72] P. Leiderer, K. Kono, and D. Rees, in *The 11th International Conference on Cryocrystals and Quantum Crystals* (2016) pp. 67–67.
[73] M. W. Cole, Phys. Rev. B **3**, 4418 (1971).
[74] K. Kajita, Surf. Sci. **142**, 86 (1984).
[75] A. Nilsson, L. G. Pettersson, and J. Norskov, *Chemical bonding at surfaces and interfaces* (Elsevier, 2011).
[76] H. Ibach, *Physics of surfaces and interfaces*, Vol. 2006 (Springer, 2006).
[77] M. I. Dykman, P. M. Platzman, and P. Seddighrad, Phys. Rev. B **67**, 155402 (2003).
[78] F. R. Bradbury, M. Takita, T. M. Gurrieri, K. J. Wilkel, K. Eng, M. S. Carroll, and S. A. Lyon, Phys. Rev. Lett. **107**, 266803 (2011).
[79] E. Kawakami, A. Elarabi, and D. Konstantinov, Phys. Rev. Lett. **126**, 106802 (2021).
[80] D. M. Pozar, *Microwave Engineering* (Wiley, 2011).
[81] D. F. Walls and G. J. Milburn, *Quantum optics* (Springer Science & Business Media, 2007).
[82] R. Bianchetti, S. Filipp, M. Baur, J. M. Fink, M. Göppl, P. J. Leek, L. Steffen, A. Blais, and A. Wallraff, Phys. Rev. A **80**, 043840 (2009).
[83] P. Krantz, M. Kjaergaard, F. Yan, T. P. Orlando, S. Gustavsson, and W. D. Oliver, Appl. Phys. Rev. **6**, 021318 (2019).
[84] M. A. Sillanpää, J. I. Park, and R. W. Simmonds, Nature **449**, 438 (2007).
[85] D. Kielpinski, C. Monroe, and D. J. Wineland, Nature **417**, 709 (2002).